

# Mechanical Implementation of a Variable-Stiffness Actuator for a Softly Strummed Ukulele

Austin B. Lawrence, Alexander N. Alspach, Darrin C. Bentivegna

**Abstract—** This research illustrates the design, implementation, and evaluation of pneumatic variable-stiffness actuator (VSA) used to strum a four-stringed ukulele with audio variability. A guitar pick is antagonistically loaded with two inflatable polydimethylsiloxane (PDMS) actuators, allowing for the independent control of both position or stiffness through the utilization of one and two PDMS solenoids, respectively. To generate smooth analog pressure signals, the bellows incorporate a controlled leak to atmospheric pressure, having synonymous properties to a low-pass filter circuit when fed a coarse pressure signal through PWM control. Experimental results illustrate a minimum to maximum stiffness range of 76 to 320 Nmm/rad, a maximum cyclical speeds of 2.04 Hz, and a stiffness change rate of 96 Nmm/rad/kPa. Additional to the VSA, alternative PDMS fabrication methods are presented to allow for complex, precise manufacturing of silicone bodies in a low-cost manner.

**Keywords—** *Soft robotics; variable-stiffness actuator; elastomers; microfluidics*

## I. INTRODUCTION

Soft machines continue to demonstrate a versatile range of useful applications, showing legitimate potential to pose new design mindsets among inventors [1]. In this paper, we focus towards the design, fabrication, and application of a variable-stiffness actuator (VSA) based on soft linear polydimethylsiloxane (PDMS) actuators. More specifically, we use an approach of vacuum-injected lost-wax casting of precision pneumatic bellows to create a VSA using two PDMS solenoids. This principle of variable stiffness in the context of actuation unveils an alternative approach to soft manipulation, which we usefully demonstrate by strumming an ukulele with variable audio intensity.

A series-elastic actuator (SEA) consists of a motor, a spring in series to an output link, and at least one sensor to measure respective displacement between the two bodies [2]. By measuring relative deformation from the motor to the output, Hooke's Law may be utilized to estimate exerted force. While VSAs follow the same operating principles as SEAs, their spring constants may be changed during operation. Because of this feature, VSAs allow for a wider range of dynamic applications by adjusting the strain limits based on the rigor of the application. Several implementations of active-stiffness control actuators have been built over the past two decades [3,4], and the field continues to be an active realm of research in the interest of

robotic manipulation [5]. VSAs are not new in concept, and neither are soft PDMS actuators [6], though these elements have not yet coexisted on this small of scale.

In the context of music, VSAs may be implemented to influence the audio amplitude at which the instrument is played, thus increasing the breadth of musical expressiveness capable from a robotic performer. While we use this device to test for entertainment, VSAs may easily be extrapolated for use into other robotic applications. Particularly in the realms of manipulation, mobility, and sensing, PDMS VSAs bear the potential to creatively solve arbitrary problems.

## II. RELATED WORK

Elastomeric robots are continuing to be exploited for their compliance in a variety of ways. As it is relatively straightforward to interface sensory hardware into the elastomeric material during the fabrication process, a wide range of data acquisition opportunities are present. Useful physical criteria, such as pressure differential [7], strain [8], temperature [9], or even opacity [10] have been measured and applied for the control of soft mechanisms. Fabrication of these systems popularly relies on a lamination technique of gradually curing silicone in layers [11], though alternative methods make use of compliant 3D-printed material [12], lost-wax casting [13], and precision soft lithography [14].

In soft actuation, new mechanisms have been implemented that rely on fluidic transmission as a primary driver. Whitney's hybrid passive-fluid rolling diaphragm is capable of efficiently transferring power through its complementary compressible air line and incompressible load-bearing water line [15]. In Mosadegh's layered soft grippers, rapid actuation is possible due to controlled distribution of strain energies from the outer membranes [16]. Though these machines do pose opportunities for feedback control, the construction remains prohibitively complex for scalability outside of the laboratory.

In musical robotics, various modes of actuation have been implemented for instrumentation. Hoffman's marimba-playing Shimon robot bears the capabilities to percussively play with technical skill, primarily thanks to its construction of high-speed linear gantries and magnetic solenoids [17]. Murphy has developed a one-stringed MechBass bass guitar robot using a stepper motor to strum the instrument, and a high-speed linear carriage to continuously fret the string for slurred musical tones [18]. Other robotic instruments, such as the McBlare bagpipe [19], Singer's GuitarBot [20], or

---

Austin B. Lawrence, Alexander N. Alspach, and Darrin C. Bentivegna are with Disney Research, Pittsburgh, PA 15213, USA.  
Austin.lawrence@disneyresearch.com

Solis' robotic saxophonist WAS-1 [21] require a devoted actuator for each individual note. With the exception of the Shimon robot, all of these systems lack a feedback mechanism to control the intensity of the musical notes, a technicality essential towards robotic musicianship [22].

### III. VARIABLE-STIFFNESS ACTUATOR DESIGN PRINCIPLES

A design analysis is provided so as to establish mathematical relationships with respect to our VSA design and performance. A simplified approach is taken to model the overall behavior of the VSA from known variable spring parameters.

#### A. Variable-Stiffness Actuator Static Analysis

A free body diagram is used to illustrate the behavior of the VSA (Figure 1). An output linkage of length  $L_l$  is grounded to a revolute output link  $A$ . Two symbolic linear springs  $k_1(p)$  and  $k_2(p)$  are antagonistically loaded at distance  $L_s$  from the output linkage's point of rotation. The springs, having variable stiffness as a function of air pressure  $p$ , will influence the spring behavior of the output linkage when pressurized.

To estimate the stiffness of the output linkage at point  $O$ , we first consider the instantaneous stiffness of a spring  $k$  based on the relationship between force  $f$  and displacement  $x$  from Hooke's Law:

$$k = \frac{\delta f}{\delta x} \quad (1)$$

As we have two springs  $k_1$  and  $k_2$  in series with one another, a net spring constant  $k_s$  may be computed:

$$\frac{1}{k_s} = \frac{1}{k_1} + \frac{1}{k_2} \quad (2)$$

From the VSA determinant analysis provided by Jafari [23], it may easily be proven that the linear spring constant  $k$  at distance  $L_l$  of the output linkage is computed as:

$$k = k_s \left( \frac{L_s}{L_l} \right)^2 \quad (3)$$

To illustrate this behavior as a torsional spring, we consider the rotational spring compliment  $k_\tau$  of Hooke's Law:

$$k_\tau = \frac{d\tau}{d\theta} \quad (4)$$

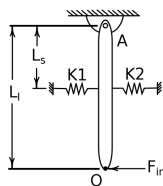


Figure 1 - A free body diagram of a revolute VSA having two antagonistic linear springs to provide stiffness at the output of link A.

and its mapping from Cartesian coordinates when linear spring  $k_s$  is deformed from small angular displacements:

$$k_\tau = k * L_l^2 \quad (5)$$

#### B. Bellows Design

With a relationship now established between the output behavior of the VSA with respect  $k_1$  and  $k_2$ , it is now of interest to design a linear PDMS actuator for the VSA system. Accordion-like bellows are designed so as to motivate actuation and stiffness in primarily one linear direction. Two design configurations are explored in this paper: one in which a bellows is designed with a single concave section, and another in which the bellows has two concave sections in series (Figure 2). Following the same philosophy as two mechanical springs in series, the double bellows configuration is anticipated to behave within the guidelines of Equation 2, having approximately half the stiffness from the single bellows configuration. To limit the amount of energy stored as strain within the PDMS, wall thickness are set to 1.2mm.

#### C. Pneumatic Low-Pass Filter Circuit

As it is challenging to design a machine solely built from compliant mechanisms, a common solution is to interface rigid bodies. A 3D printed block is bound to the PDMS bellows using a silicone epoxy (Smooth-on Sil-Poxy). Polyjet™ 3D printing allows for two materials to be printed simultaneously, which we use to incorporate a compliant seal into the otherwise rigid inlet port. With a large enough clamping force and utilization of a high-viscosity lubricant for sealing the bellows assembly to its pressure source (DuPont Krytox), no uncontrolled leakage is detectable.

The mounting block also includes features for enabling a controlled leak, which serves as a mechanism for smoothing the PWM pressure signal (Figure 2). An adjustable set screw is used to regulate flow rate of escaping air, also influencing the pressure of the bellows. In providing a passive path to atmospheric pressure through the low-pass filter, bi-directional position control is possible with one solenoid. As this configuration is equivalent in operation to an electrical RC circuit, Mosadegh's framework microfluidic circuitry may serve as a useful starting point in estimating time constants with respect to computed resistance and capacitance values [24].

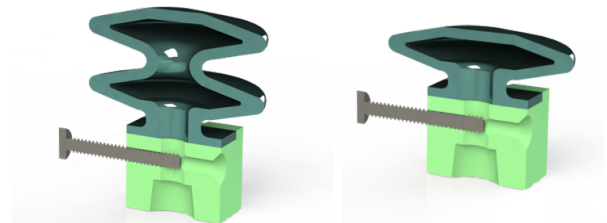


Figure 2 – (left) An illustration of a double stage bellows assembled into a pneumatic low-pass filter base. (right) A single bellows configured into the same base.

#### IV. FABRICATION

The PDMS bellows are fabricated using a custom liquid silicone injection molder and lost-wax casting techniques. An Objet Connex260 PolyJet 3D printer [25] is used to fabricate smooth molds (VeroClear) for casting both the PDMS bellows and their paraffin wax cores. The molds are placed in a temperature controlled oven at 50°C for at least five hours before being used, so as to resist any inhibition of the PDMS vulcanization process that may occur as a result of incompletely cured PolyJet material.

##### A. Wax Cores

The wax cores are manufactured by gradually dripping molten wax into the open face of a mold mounted in a centrifuge. Paraffin wax is heated to a temperature of 65°C and drawn into a syringe for precise administration. A PTFE lubricant (DuPont Teflon Silicone) is lightly sprayed along the inside of the mold as a releasing agent, and a stainless steel rod affixed to the center for positioning the core in a later step. The wax mold is spun at approximately 1500 RPM while wax is gradually injected. When wax begins to overflow at high RPMs, the rotational velocity is gradually reduced to zero while ensuring that the mold remains overflow. Such a technique is not necessary for large, smooth molds, though it is useful for maximizing surface detail in precision parts in one single operation. The wax core is allowed to solidify at room temperature for 20 minutes and is subsequently removed from the mold.

##### B. PDMS Injection Molding

The mold for casting PDMS is prepared with a mold release agent (Mann Ease Release 200) and the wax core is oriented in the mold using the stainless steel rod for positioning. A batch of PDMS (Dragonskin-30) is mixed and then degassed inside a syringe for 20 minutes. The syringe and PDMS mold are placed into a custom leadscrew-driven injection molder and primed until liquid silicone reaches a three-way valve (Figure 3). Vacuum is pulled from the mold to ensure the complete omission of trapped air bubbles during the injection process. After sufficiently pulling vacuum, the three-way valve is switched to allow silicone to flow into the mold, and the leadscrew driven by hand until incompressibility is registered. When the appropriate amount of silicone has flown, the cast is cured at 50°C for 45 minutes and is subsequently released. It is then heated to 65°C, allowing the molten wax to melt and drain from the cast.

#### V. EXPERIMENT

In this section, we describe the experimental methods used in quantifying the physical behavior of the silicone bellows, and the results that come from applying our VSA to the strumming of an ukulele.

##### A. Design Overview

An apparatus has been built for the purpose of strumming a secured ukulele with variable audio intensity (Figure 4). A linear carriage may reciprocate in a perpendicular direction to the guitar strings to replicate a

strumming motion. On the carriage is a revolute VSA with affixed picking mechanism. PDMS bellows are antagonistically mounted offset from the revolute axis of the guitar pick in order to create the variable-stiffness component of the VSA when pressurized (Figure 5). Also included on the carriage is an optical encoder (Yumo A6B2), a pressure transducer (Freescale MPX5500DP), PTFE linear bearings, and compressed air hookups.

A three-way solenoid manifold (X-Valve) is mounted onto a compliant 3D-printed structure (Tango+) for purposes of dampening vibrations resultant from solenoid PWM. To further reduce sound caused by the solenoids, the manifold assembly is placed within an insulated acrylic case. An Arduino Due microcontroller is used for interfacing to a computer through rosserial in conjunction with ROS. The microcontroller is used to relay sensory information measured from the optical encoder and pressure transducer, providing sensor readings and digital writes at 100Hz. A 3.3V 40Hz PWM signal is run through a MOSFET array to provide a 12V signal to the PDMS solenoids for producing an analog pressure signal. Lastly, an H-Bridge (Cytron 13A) is powered through an external source and used to drive the gear motor coupled to the reciprocating carriage.

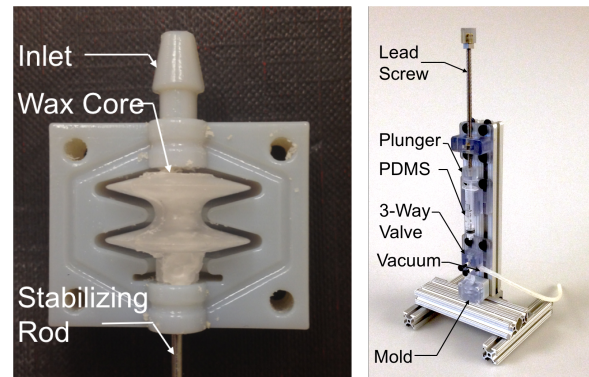


Figure 3 - (left) A wax core centered within the PDMS cast, ready for injection molding. (right) A leadscrew-driven injection molder having a 3D-printed three-way valve for degassing molds prior to injecting PDMS.

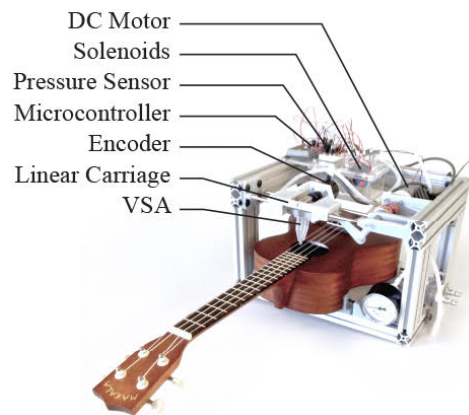


Figure 4 – An annotated image of a softly strummed ukulele using a VSA.

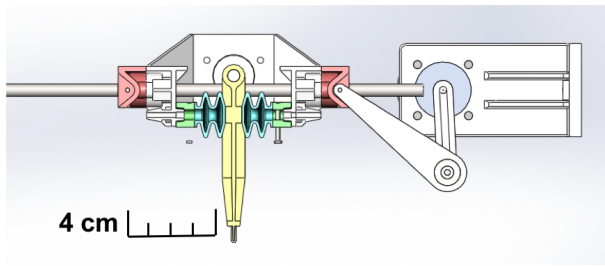


Figure 5 – A cross sectional view of the VSA. The PDMS bellows (blue) may be inflated to exert force onto the output link (yellow). A DC gear motor creates reciprocating linear motion of the carriage.

### B. Control

Two schemes are explored to control the behavior of the VSA: one mode in which bi-directional position feedback control of the output shaft is possible, and a second mode in which the stiffness of the output joint is adjusted while holding position constant. To implement both of these control methods, two different solenoid configurations are used (Figure 6).

In the position control configuration, a positive pressure source is connected to the common port of solenoid  $S_1$  and subsequently distributing pressurized air to the respective bellows  $C$  and grounded low-pass filters  $R$ . PWM duty cycles are determined using PD control from encoder feedback. In the stiffness configuration,  $S_2$  regulates the pressure leading into the common port of  $S_1$ .  $S_1$  is held at a 50% PWM to evenly distribute output pressures. Prior to implementing either scenario, the value of  $R$  is adjusted through the setscrew illustrated in Figure 2 until the output link is perpendicular to the ukulele strings.

As no form of strain measurement is present within this VSA configuration, prior experimental analysis of each bellows is necessary in order to achieve open-loop stiffness control. A spring characterization, having drawn a relationship between stiffness  $k(p)$  and  $p$ , is used as a means of estimating stiffness in real time. With this relationship assumed known, PD control is used to regulate  $p_{sense}$  by adjusting duty cycle values in  $S_2$ .

Though two solenoids are used in this paper to regulate stiffness, truly only one is necessary. As shown in Figure 6,  $S_1$  effectively functions as a tee-valve, evenly distributing pressure between two lines. Provided that pressure is equally delivered to each bellows using a passive component, only  $S_2$  is necessary to adjust the magnitude of the pressure  $p$  when using stiffness control. Two solenoids are used in this setup to avoid manual reconfiguration when switching between position control and stiffness control.

### C. VSA System Identification

In order to quantify the output stiffness of the VSA, knowledge of the spring behavior with respect to pressure is necessary. To do this, both the single and double bellows are mounted into a force-displacement machine and measured for spring response with respect to pressure. A stress-strain machine (Mark-10 ESM301) is used to gradually apply compression along the center axis of the bellows at a rate of 10 mm/s. A strain gauge (AmCells

STL-25) measures the force exerted onto the bellow. With each compression experiment, the pressure of the bellows is incremented by 3.5 kPa.

Stiffness is calculated with respect to displacement using Equation 1 and linearized in Figure 8. Between pressure ranges of 0 to 35 kPa, the single bellows' stiffness increased from 0.98 N/mm to 2.25 N/mm, whereas the double bellows increased from 0.57 N/mm to 0.88 N/mm. Using this figures with Equation 5 and  $L_1$  of 80mm, the stiffness range of the VSA is 76 and 320 Nmm/rad for a double bellows over a 0 to 35 kPa range. Buckling was prevalent in the double bellows design at higher pressures, as reflected in the rapid drops of spring stiffness in Figure 9.

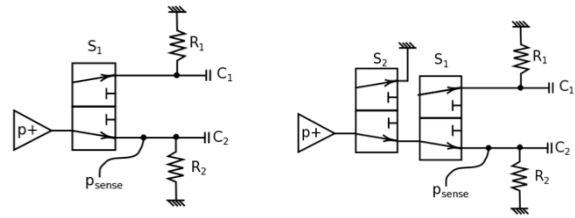


Figure 6 - (left) The pneumatic circuit configuration for position control. (right) A pneumatic circuit for stiffness control, with  $S_1$  held at 50% PWM duty cycle.



Figure 7 - The experimental setup used for performing force-displacement tests. Bellows are mounted onto a removable test jig and measured for spring deformation.

### Force-Displacement Spring Stiffnesses

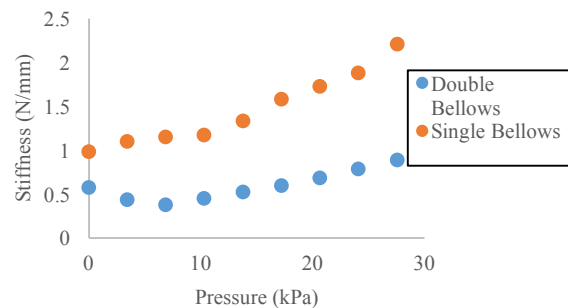


Figure 8 – A double and single bellows' spring constant from a linear fit of force-displacement data.

## Spring Constants with Respect to Pressure and Displacement

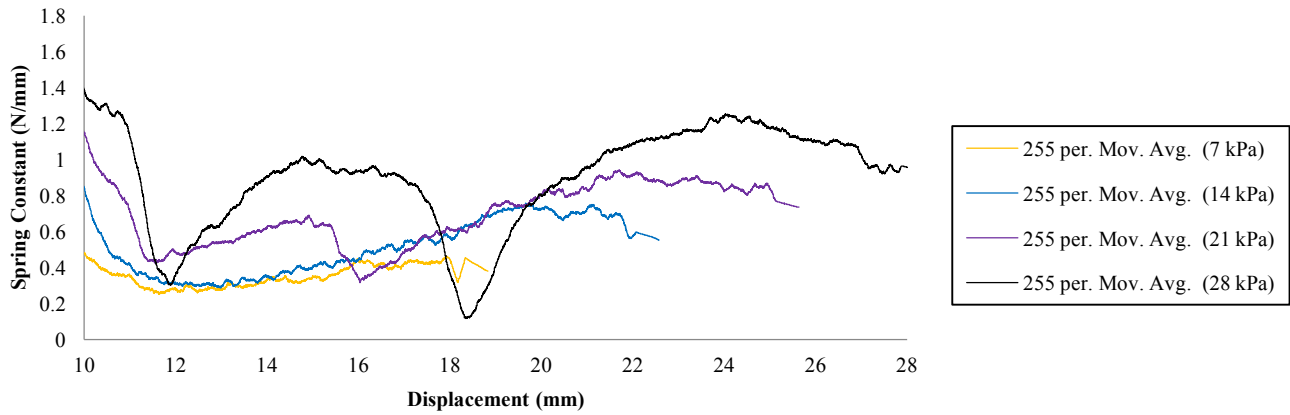


Figure 9 - Calculated spring constants when performing a force-displacement test on a double bellows. At higher pressures, the double bellows buckled under load, as reflected in the graph's deviations.

### D. Position Control

In the interest of assessing the dynamic behavior of the VSA, a stress test for positional accuracy was conducted to reveal limitations in speed. A reference sine wave is generated having function  $\theta(t) = 10 * \sin(0.4\pi t^2)$ . Upon adjusting PD values of the controller to be critically damped, the trajectory of the end effector is monitored when passed the reference sine wave function. Two pressure signals are examined: one at 35 kPa, and another at 20 kPa (Figure 10). A positioning error of 20% becomes apparent at 2.04 Hz and 1.67 Hz for each respective pressure.

### E. Stiffness Control

As an application, the VSA is configured to strum an ukulele at varying levels of audio intensity through the adjustment of stiffness. Using the same stiffness adjustment protocol as found in the Experiment section, the instrument is strummed at a 2 Hz frequency with double bellows configured into the VSA. Audio data is captured with a computer microphone at 0.5 meters from the strings. The audio signal is subsequently converted into the frequency domain using a Fast Fourier Transform and threshold limits of 180 Hz and 460 Hz, which reflect the range in pitches anticipated from a properly tuned ukulele. The peak decibel levels within this range are measured with respect to VSA pressure (Figure 11). The minimum and maximum audio amplitude of 78 dB and 88 dB, respectively, were measured over the VSA's pressures of 0 kPa and 38 kPa.

## VI. DISCUSSION

In the force-displacement tests, a relationship between spring stiffness, air pressure, and displacement appear to exist, though the relationships were not as strong as anticipated. As shown in Figure 8, a clear difference in the behavior of the single bellows versus the double bellows is apparent, with the single bellows having a very linear relationship between force and displacement when pressure is held constant. In the case of the double bellows, buckling

was observed during testing of higher pressures, as a possible outcome of imperfections of the manufacturing process, asymmetric loading of the stress-strain machine, or simply due to the overall length of the soft actuator.

### Sinusoidal Position Response

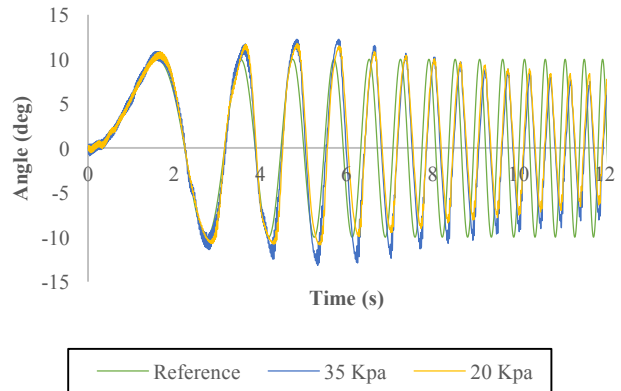


Figure 10 - Positional accuracy as a function of input pressures 35 kPa and 20 kPa. At higher frequencies, positional error is exaggerated with lower operating pressures.

### Ukulele Sound Intensity Vs. Pressure

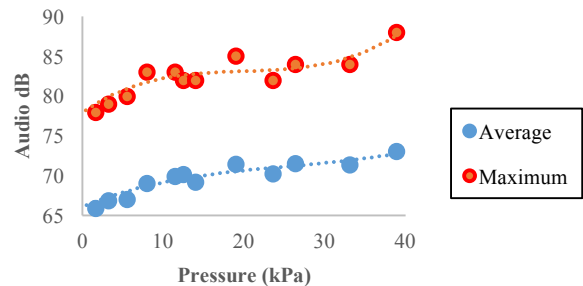


Figure 11 - Measured audio decibel intensity with respect to changes of the VSA's spring stiffness.

Despite the issue of buckling, the behaviors of the bellows follow trends illustrated in the Variable-Stiffness Actuator Design Principles section. At 38 kPa, the double bellows was measured to have 2.19 times the extension from the single bellows at the same pressure. Under these same conditions, the linear spring constant was found to be 2.30 times larger for the smaller bellows, suggesting that bellows with multiple concave-convex sections in series have similar operating principles to mechanical springs in series.

Nonlinearities in stiffness as pressure increased were also apparent, as shown in Figure 9. Though buckling does pose the risk of misrepresenting stiffness about a linear axis, an extrapolated trend would appear to exist to suggest stiffness to increase with pressure. Such an assumption is appropriate based on the nonlinear behavior of compressible gasses at higher pressures. Higher pressures were not explored in this paper due to the relatively delicate requirements of playing an ukulele. As the wall thickness of the PDMS bellows were intentionally designed to be thin, high pressures would have increased the likelihood of rupture. Methods to reinforce the PDMS, by incorporating fiberglass into the structure, or following the design principles of a McKibben actuator [26], may be a suitable approach for increasing the rigor of performance capable from the bellows.

Though implementing the static analysis model found in the Variable-Stiffness Actuator Static Analysis section is viable for estimating the output spring behavior of the VSA, it is believed that spring stiffness calibration from displacements of a point mass pendulum experiment may be more reliable. A mass of known inertia may be attached to the output linkage and allowed to move as a result of spring influence, as well as an outside force stimulus. By recording the displacement of the point mass, a FFT can be used to express the signal in the frequency domain, thus revealing natural frequencies of the VSA. By undergoing a simple conversion found in harmonic springs, a spring constant may be determined with respect to the pressure supplied. Such an implementation would ensure spring calibration of the assembled system, thus omitting the need to remove any bellows for assessment.

Lastly, the decisions made in the overall design of the VSA proved to play a significant role in the overall performance. The limited orifice size of the X-Valve at 1.6mm implies an area of high viscous losses, even at lower pressures. In light of this, and apparent in Figure 10, the rate at which bellows pressure may be changed is reduced, thus inhibiting its ability to make rapid adjustments in stiffness or position. Sourcing a larger solenoid and hose fittings will ensure rapid response of the VSA, making the device more applicable for dynamic applications.

## VII. CONCLUSION AND FUTURE WORK

We have developed a derivation of a VSA that utilizes PDMS bellows to tune stiffness using an input pressure signal. A method is presented to provide estimations for the spring behavior of complex pressurized hyperelastic structures and used for dictating the design of the PDMS

bellows. An alternative approach to PDMS fabrication is presented using vacuum lost-wax casting techniques. Multiple testing protocols are implemented in order to quantify the physical behavior of the VSA under various conditions. Lastly, we have demonstrated its application through measurable differences in audio amplitude when strumming an ukulele.

Pressure limits faced by the bellows, as well as the available flowrate, proved to be the biggest restrictions in achieving a more diverse range of performance from the VSA. Special initiatives to amend these issues, using larger orifices, or reinforcing the elastomer, are likely to have a positive effect on the functional capabilities for the VSA.

For the future, we would like to continue the initiative in VSAs by increasing the range in performance capable from such devices, as well as their self-identification. Additionally, it is of interest to continue towards full autonomy of the robotic ukulele by incorporating fluidic structures with embedded components for fretting the instrument.

## ACKNOWLEDGEMENTS

We would like to thank Dr. Yong-Lae Park and Jackson Wirekoh of the Carnegie Mellon Soft Machine Laboratory for their insight and equipment when conducting force-displacement tests.

## REFERENCES

- [1] Yao, L., Niyama, R., Ou, J., Follmer, S., Della Silva, C., & Ishii, H. (2013). PneuUI: Pneumatically Actuated Soft Composite Materials for Shape Changing Interfaces. *Proceedings of the 26th Annual ACM Symposium on User Interface Software and Technology - UIST '13'*
- [2] Pratt, G. A., & Williamson, M. M. (1995). Series Elastic Actuators. *Proceedings 1995 IEEE/RSJ International Conference on Intelligent Robots and Systems. Human Robot Interaction and Cooperative Robots*, 1, 399–406. doi:10.1109/IROS.1995.525827
- [3] Salisbury, J. (1980). Active stiffness control of a manipulator in cartesian coordinates. *1980 19th IEEE Conference on Decision and Control Including the Symposium on Adaptive Processes*, 19, 95–100. doi:10.1109/CDC.1980.272026
- [4] Grossard, M., Moreau, S., & Poinot, T. (2015). Sensorless Force / Position Control of a Single-Acting Actuator Applied to Compliant Object Interaction, *62(6)*, 3651–3661.
- [5] Churchill, C. B., Shahan, D. W., Smith, S. P., Keefe, A. C., & Mcknight, G. P. (2016). Dynamically variable negative stiffness structures, (February), 1–7.
- [6] Hirose, S., & Umetani, Y. (1978). The development of soft gripper for the versatile robot hand. *Mechanism and Machine Theory*, *13(3)*, 351–359. doi:10.1016/0094-114X(78)90059-9
- [7] Vazquez, M., Brockmeyer, E., Desai, R., Harrison, C., & Hudson, S. (2015). 3D Printing Pneumatic Device Controls with Variable Activation Force Capabilities.
- [8] Vogt, D., Menguc, Y., Park, Y., & Wehner, M. (2013). Progress in Soft, Flexible, and Stretchable Sensing Systems. *Biorobotics.Harvard.Edu*, 0–1. Retrieved from [http://biorobotics.harvard.edu/pubs/2013/contrib/DVogt\\_2013ICRA.pdf](http://biorobotics.harvard.edu/pubs/2013/contrib/DVogt_2013ICRA.pdf)
- [9] Z. Hu, X. Zhang, and Y. Li, "Synthesis and application of modulated polymer gels," *Science*, vol. 269, pp. 525–527, 1995.
- [10] A. Suzuki and T. Tanaka, "Phase transition in polymer gels induced by visible light," *Nature*, vol. 346, pp. 345–347, 1990.
- [11] Cham, J. G., Bailey, S. a, Clark, J. E., Full, R. J., & Cutkosky, M. R. (2002). Fast and Robust: Hexapedal Robots via Shape Deposition

- Manufacturing. *The International Journal of Robotics Research*, 21(10), 869–882. doi:10.1177/0278364902021010837
- [12] Kim, J., Alspach, A., & Yamane, K. (2015). 3D Printed Soft Skin for Safe Human-Robot Interaction.
- [13] Marchese, A. D., Katzschmann, R. K., & Rus, D. (2015). A Recipe for Soft Fluidic Elastomer Robots. *Soft Robotics*, 2(1), 7–25. doi:10.1089/soro.2014.0022
- [14] Mosadegh, B., Mazzeo, A. D., Shepherd, R. F., Morin, S. a., Gupta, U., Sani, I. Z., ... Whitesides, G. M. (2014). Control of soft machines using actuators operated by a Braille display. *Lab Chip*, 14(1), 189–199. doi:10.1039/C3LC51083B
- [15] Whitney, J. P., Glisson, M. F., Brockmeyer, E. L., & Hodgins, J. K. (2014). A low-friction passive fluid transmission and fluid-tendon soft actuator. *2014 IEEE/RSJ International Conference on Intelligent Robots and Systems*, 2801–2808. doi:10.1109/IROS.2014.6942946
- [16] Mosadegh, B., Polygerinos, P., Keplinger, C., Wennstedt, S., Shepherd, R. F., Gupta, U., ... Whitesides, G. M. (2014). Pneumatic Networks for Soft Robotics that Actuate Rapidly. *Advanced Functional Materials*, 24(15), 2163–2170. doi:10.1002/adfm.201303288
- [17] Weinberg, G., Raman, A., & Mallikarjuna, T. (2009). Interactive jamming with Shimon: A social robotic musician. *Human-Robot Interaction (HRI), 2009 4th ACM/IEEE International Conference on*, 233–234. doi:10.1145/1514095.1514152
- [18] Mcvay, J., Carnegie, D. a, Murphy, J., & Kapur, A. (2011). MechBass: A Systems Overview of a New Four-Stringed Robotic Bass Guitar.
- [19] Dannenberg, R. B., Brown, B., Zeglin, G., & Lupish, R. (2005). McBlare: A Robotic Bagpipe Player. *Proceedings of the 2005 International Conference on New Interfaces for Musical Expression (NIME-05)*, 80–84. Retrieved from [http://www.nime.org/proceedings/2005/nime2005\\_080.pdf](http://www.nime.org/proceedings/2005/nime2005_080.pdf)
- [20] Singer, E., Larke, K., & Bianciardi, D. (2003). LEMUR GuitarBot: MIDI Robotic String Instrument. *Proceedings of the 2003 Conference on New Interfaces for Musical Expression (NIME-03)*, 188–191.
- [21] Solis, J. et. al. (2010). Development of the Anthropomorphic Saxophonist Robot WAS-1: Mechanical Design of the Simulated Organs and Implementation of Air Pressure. *Advanced Robotics Journal* 24
- [22] Weinberg, G., & Driscoll, S. (2006). Toward Robotic Musicianship. *Computer Music Journal*, 30(4), 28–45. doi:10.1162/comj.2006.30.4.28
- [23] Jafari, A., Vu, H. Q., & Iida, F. (2015). Determinants for Stiffness Adjustment Mechanisms. *Journal of Intelligent & Robotic Systems*, (January). doi:10.1007/s10846-015-0253-8
- [24] Mosadegh, B., Kuo, C.-H., Tung, Y.-C., Torisawa, Y., Bersano-Begey, T., Tavana, H., & Takayama, S. (2010). Integrated elastomeric components for autonomous regulation of sequential and oscillatory flow switching in microfluidic devices. *Nature Physics*, 6(6), 433–437. doi:10.1038/nphys1637
- [25] Stratasys. (2014) Object260 connex. [Online]. Available: <http://www.stratasys.com/3d-printers/design-series/objet260-connex>
- [26] Chou, C.-P., & Hannaford, B. (1996). Measurement and modeling of McKibben pneumatic artificial muscles. *TRA (Transactions on Robotics and Automation)*, 12(1), 90–102. doi:10.1109/70.481